

Received November 7, 2020, accepted November 25, 2020, date of publication December 2, 2020,
date of current version December 14, 2020.

Digital Object Identifier 10.1109/ACCESS.2020.3041292

Multi-Objective Trajectory Planning Method for a Redundantly Actuated Parallel Manipulator Under Hybrid Force and Position Control

JIANBIN FENG^{id}, TIEJUN LI^{id}, (Member, IEEE), MING HAN^{id},
KAIWEN ZHENG^{id}, AND DONG YANG^{id}

School of Mechanical Engineering, School of Mechanical Science and Engineering, Hebei University of Technology, Tianjin 300131, China

Corresponding author: Dong Yang (y__dong@126.com)

This work was supported in part by the National Natural Science Foundation of China (NSFC) under Grant U1813222, in part by the Hebei Key Research and Development Plan under Grant 19211816D, and in part by the Postgraduate Innovation Funding Project of Hebei Province under Grant CXZZSS2020026.

ABSTRACT A multi-objective trajectory planning method for redundantly actuated parallel manipulator under hybrid force and position control is proposed considering the coordination of its driving forces. Combining inverse kinematics analysis, the driving force coordination of the manipulator is analyzed using the virtual work principle. On this basis, the B-spline curve is used to plan the motion trajectory of the end-effector of the manipulator in the Cartesian space. Subsequently, the driving force coordination, total motion time, and maximum absolute value of the jerk impulse of the actuator are defined as objective functions, and a multi-objective optimization problem is solved using the multi-objective particle swarm algorithm (MOPSO). Finally, the potential optimal solution is selected by constructing a comprehensive optimal evaluation function. The trajectory simulation results verify that the trajectory planning method is effective and universal.

INDEX TERMS Redundantly actuated parallel manipulator, trajectory planning, driving force coordination, multi-objective optimization.

I. INTRODUCTION

Redundantly actuated parallel robots have advantages of conventional parallel robots such as high carrying capacity and high rigidity. With the introduction of actuation redundancy in a manipulator, its kinematic singularities [1] can be effectively reduced, and the internal loading of the actuators can be minimized [2]. In addition, the dexterity [3] and dynamic performance [4] can be improved. These advantages make redundantly actuated parallel manipulators suitable for building construction. The number of linearly independent drives in this type of manipulator is greater than the number of independent motion degrees of freedom of the manipulator. Compared with the conventional non-redundantly actuated parallel manipulator, the coupling between the drives of a redundantly actuated parallel manipulator is more complicated and requires higher coordination [5].

The associate editor coordinating the review of this manuscript and approving it for publication was Zheng Chen^{id}.

During operations for example, a manipulator needs to transport workpieces from the initial pose to the target pose to complete the installation work, which can be considered a point-to-point motion trajectory planning problem [6]. By rationally planning the trajectory, a manipulator can achieve the required performance while meeting the task requirements. The stability and continuity of the trajectory are important indicators of the performance of the manipulator. Therefore, smooth trajectories in terms of the displacement, velocity, acceleration, and acceleration ratio of the joints and end-effectors are displayed in the form of continuous curves in motion, which has been the focus of research in trajectory planning [7]–[10]. Considering the work efficiency, Liu *et al.* applied 4-3-3-4-degree polynomial interpolation along with an improved particle swarm algorithm to obtain a time-optimal trajectory [11]. The authors of [12] employed a combination of multiple spline planning in the Cartesian space and multiple B-spline planning in the joint space to plan a smooth trajectory with an optimal motion time. Kucuk obtained the time-optimal trajectory using the

cubic spline curve, based on which the first and last nodes of the trajectory were interpolated using a seventh-degree polynomial, and combined with the particle swarm algorithm, a smooth trajectory was generated with an optimal motion time [13].

With the advancements in the field of robotics, in order to meet the requirements of a variety of practical applications, multi-objective trajectory planning has attracted considerable research attention [14]–[18]. For example, Huang *et al.* applied the 5th-order B-spline to perform trajectory interpolation in the joint space and then optimized the result using the elitist non-dominated sorting genetic algorithm (NSGA-II) to obtain a comprehensive optimal trajectory in terms of the time and jerk. In addition, two performance indicators were proposed to evaluate the effectiveness of the Pareto optimal front and select the optimal solution [19]. Recently, Dong *et al.* used a B-spline curve to parametrically express a trajectory in the Cartesian space by considering the working accuracy of the end-effector. Subsequently, an improved immune cloning algorithm was proposed to solve the multi-objective optimization problem, and the potential optimal trajectory was obtained using an average optimal solution method [20]. Although there are many trajectory planning studies, there are few on redundantly actuated parallel manipulators. The authors of [21] proposed a dynamic trajectory planning method for a planar two-degree-of-freedom redundant-drive suspension-cable parallel manipulator. Pham and Stasse used a dynamic programming method to obtain a time-optimal trajectory with the finite element approximation of the Hamilton–Jacobi–Bellman equation [22].

However, there is no trajectory optimization research on the driving force coordination of redundantly actuated parallel manipulators, despite the significant advances in robot trajectory planning research. Therefore, a trajectory planning method is proposed in this paper to meet the characteristics and actual work requirements of redundantly actuated parallel manipulators under a hybrid force and position control. First, a quintic B-spline curve is used to parameterize all the trajectories. On this basis, the multi-objective particle swarm algorithm (MOPSO) is applied to optimize the driving force coordination, movement time, and jerk. Finally, a comprehensive optimal method is proposed to obtain the optimal trajectories of the end-effector and joints of the manipulator.

The rest of this paper is organized as follows: In Section 2, the redundantly actuated parallel manipulator and its trajectory planning strategy are introduced, and the inverse kinematic model and dynamic model are analyzed. In Section 3, the trajectory generation method is formulated. In Section 4, a mathematical model of the multi-objective optimal trajectory is established, and the MOPSO is introduced. Section 5 presents the simulation of the trajectory planning problem and the obtained results. Finally, in Section 6, the conclusions are presented.

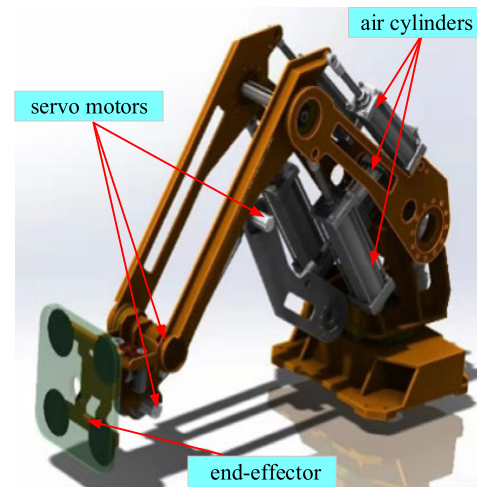


FIGURE 1. Redundantly actuated parallel manipulator.

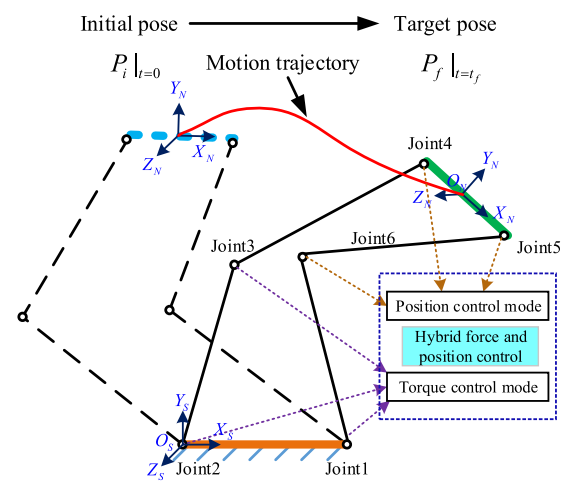


FIGURE 2. Schematic of the trajectory planning.

II. REDUNDANTLY ACTUATED PARALLEL MANIPULATOR AND ITS TRAJECTORY PLANNING STRATEGY

Redundantly actuated parallel manipulators are mainly used in building construction and can be used for installing curtain walls or panels, as shown in FIGURE 1. The main body of this manipulator has six bars, and its six joints are driven by three servo motors and three air cylinders to achieve a hybrid force and position control [23], [24]. During the motion of the manipulator, the three servo motors control the pose of the end-effector, and the three cylinders help adjust each driving torque and internal loading of the actuators, thus ensuring that the manipulator has a three-degrees-of-freedom motion in the working space and driving force-coordinated control ability.

To ensure that the motion of the end-effector is accurate and stable, and considering the simple characteristics of the inverse kinematics, the motion trajectory of the end-effector is planned in the Cartesian space. FIGURE 2 shows a simple illustration of the trajectory planning assignment. Joints 1, 2, and 3 in the force control mode are defined as redundantly

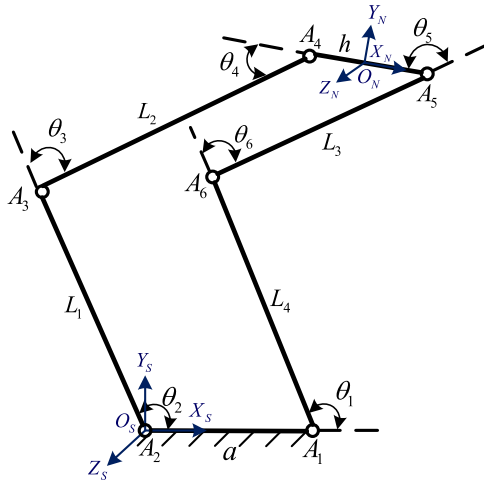


FIGURE 3. Geometric structure of a redundantly actuated parallel manipulator.

actuated joints, whereas Joints 4, 5, and 6 in the position control mode are defined as non-redundantly actuated joints. Evidently, the motion trajectory of the end-effector is essentially determined by the motions of the three joints that are in the position control mode, and the various performance improvements of the manipulator are closely linked to the adjustment of the three joints that are in the torque control mode. Therefore, the kinematics and dynamic analyses of the manipulator are significant preconditions to meet the requirements of the trajectory planning task.

A. INVERSE KINEMATICS ANALYSIS OF THE MANIPULATOR

The manipulator can be simplified as a six-bar manipulator, as shown in FIGURE 3. To facilitate the analysis, a fixed coordinate system {S} was established at the first joint, and a moving coordinate system {N} was established at the center of the end-effector. The motion trajectory of the end-effector can be described using the pose parameter (x0, y0, gamma0). Accordingly, the generalized coordinates that define the motion of the mechanism in the space are:

$$\mathbf{q} = [x_0 \ y_0 \ \gamma_0]^T, \tag{1}$$

where [x0 y0]^T is the position vector of the origin ON of the moving coordinate system in the fixed coordinate system {S}, and gamma0 is the Euler angle of the mobile coordinate system {N} in the fixed coordinate system {S}.

Assuming that the joint angle of each driving joint is theta_i, the inverse kinematics model of the joints can be obtained using the closed vector method, which can be simplified as:

$$\theta_i = f_i(x_0, y_0, \gamma_0) \quad (i = 1, 2, \dots, 6), \tag{2}$$

where f_i is the function of the inverse kinematics model.

Assuming that the generalized velocity coordinate describing the motion of the manipulator is q-dot = [x-dot_0 y-dot_0 gamma-dot_0], the

angular velocity of each joint under this coordinate can be obtained by calculating the first derivative of (1).

$$\begin{cases} \dot{\theta}_1 \\ \dot{\theta}_2 \\ \dot{\theta}_3 \end{cases} = \mathbf{J}_R \cdot \dot{\mathbf{q}} \\ \begin{cases} \dot{\theta}_4 \\ \dot{\theta}_5 \\ \dot{\theta}_6 \end{cases} = \mathbf{J}_N \cdot \dot{\mathbf{q}}, \tag{3}$$

where JR and JN are the velocity Jacobian matrices of the redundantly and non-redundantly actuated joints, respectively. According to (2), the acceleration and jerk of each joint can be obtained as follows.

$$\begin{aligned} [\ddot{\theta}_1 \ \ddot{\theta}_2 \ \ddot{\theta}_3 \ \ddot{\theta}_4 \ \ddot{\theta}_5 \ \ddot{\theta}_6]^T &= \frac{\partial \mathbf{J}_v}{\partial \mathbf{q}} \cdot (\dot{\mathbf{q}})^2 + \mathbf{J}_v \cdot (\ddot{\mathbf{q}}) \\ [\ddot{\theta}_1 \ \ddot{\theta}_2 \ \ddot{\theta}_3 \ \ddot{\theta}_4 \ \ddot{\theta}_5 \ \ddot{\theta}_6]^T &= \frac{\partial \mathbf{J}_a}{\partial \mathbf{q}} \cdot (\dot{\mathbf{q}})^3 + \mathbf{J}_a \cdot (3 \cdot \dot{\mathbf{q}} \cdot \ddot{\mathbf{q}}) \\ &\quad + \mathbf{J}_v \cdot \ddot{\mathbf{q}}, \end{aligned} \tag{4}$$

where Jv = [JR JN]^T is the velocity Jacobian matrix of each joint in the generalized coordinates, Ja = dJv/dq.

B. DYNAMIC ANALYSIS OF THE MANIPULATOR

A manipulator is mainly affected by gravity, external loads, inertial forces, and driving forces during motion. Therefore, the virtual power balance equation of the manipulator is established by the principle of virtual work to establish a dynamic model. To simplify the analysis, the following calculations are performed under generalized coordinates q = [x0 y0 gamma0]^T.

Taking the velocity Jacobian matrix of the moving member of the manipulator as Ji, the velocity of each moving member can be expressed as:

$$\mathbf{v}_i = \mathbf{J}_i \cdot \dot{\mathbf{q}}, \tag{5}$$

Taking the velocity Jacobian matrices of the non-redundantly and redundantly actuated joints as JNi and JRj, respectively, the velocities of the two types of joints can be expressed as:

$$\begin{aligned} \mathbf{v}_{Ni} &= \mathbf{J}_{Ni} \cdot \dot{\mathbf{q}} \quad i = 1 - 3 \\ \mathbf{v}_{Rj} &= \mathbf{J}_{Rj} \cdot \dot{\mathbf{q}} \quad j = 1 - 3, \end{aligned} \tag{6}$$

According to (3), JN = [JN1 JN2 JN3] and JR = [JR1 JR2 JR3]. Taking the velocity Jacobian matrix of the component of the manipulator under an external load force as JFi, the velocity of this component can be expressed as:

$$\mathbf{v}_{Fi} = \mathbf{J}_{Fi} \cdot \dot{\mathbf{q}}, \tag{7}$$

According to D'Alembert's principle, the inertial forces and moment of the moving members of the manipulator can be expressed as follows.

$$-\mathbf{m}_i \cdot \mathbf{a}_i = -\mathbf{M}_i \cdot \ddot{\mathbf{q}} - \mathbf{C}_i \cdot \dot{\mathbf{q}}, \tag{8}$$

where mi denotes the inertia of each moving member, ai denotes the acceleration vector of each moving member, Mi

denotes the acceleration term coefficient, and C_i denotes the velocity term coefficient.

Suppose Q_i denotes the gravity vector acting on each moving member of the manipulator, F_{Fi} denotes the external force borne by each load member, τ_{Ni} denotes the driving force of the non-redundantly actuated joint, and τ_{Rj} denotes the driving force of the redundantly actuated joint.

Based on the equilibrium equation of virtual work, a virtual work balance equation for the manipulator is established as follows.

$$\sum v_i^T \cdot (-m_i \cdot a_i + Q_i) + \sum v_{Fi}^T \cdot F_{Fi} + \sum_{i=1}^3 v_{Ni}^T \cdot \tau_{Ni} + \sum_{i=1}^3 v_{Rj}^T \cdot \tau_{Rj} = 0, \quad (9)$$

Substituting (5)-(8) into (9) yields:

$$\sum J_i^T \cdot (-M_i \cdot \ddot{q} - C_i \cdot \dot{q} + Q_i) + \sum J_{Fi}^T \cdot F_{Fi} + \sum_{i=1}^3 J_{Ni}^T \cdot \tau_{Ni} + \sum_{i=1}^3 J_{Rj}^T \cdot \tau_{Rj} = 0, \quad (10)$$

If the generalized inverse theory of the matrix is adopted, the driving force can be used as the minimum two-norm solution to optimize the distribution, and then $\tau_R = [\tau_{R1} \ \tau_{R2} \ \tau_{R3}]^T$ as an independent variable and $\tau_N = [\tau_{N1} \ \tau_{N2} \ \tau_{N3}]^T$ as dependent variables. Accordingly, further formulating (10) yields:

$$\tau_N = (J_N)^{-T} \cdot \left[\begin{array}{c} \sum J_i^T \cdot M_i \cdot \ddot{q} + \sum J_i^T \cdot C_i \cdot \dot{q} \\ -\sum J_i^T \cdot Q_i + \sum J_{Fi}^T \cdot F_{Fi} \end{array} \right] - (J_N)^{-T} (J_R)^T \cdot \tau_R \quad (11)$$

Assuming that the driving force changes in the redundant and non-redundant drives are $\Delta\tau_R$ and $\Delta\tau_N$, respectively, it can be obtained from (11) that:

$$\Delta\tau_N = -(J_N)^{-T} (J_R)^T \cdot \Delta\tau_R, \quad (12)$$

According to the matrix analysis theory, the norm $\|(J_N)^{-T} (J_R)^T\|$ reflects the magnification of the generalized length of the driving force adjustment when mapping the redundantly actuated force space to the non-redundantly actuated force space. It represents the driving force adjustment capability of the redundantly actuated joint with respect to the non-redundantly actuated joint, and its magnitude is related to the motion trajectory of the end-effector of the manipulator. When the manipulator is under a hybrid force and position control, an excessive adjustment will lead to an increase in the adjustment error, which will cause the manipulator to generate greater internal forces, causing greater fluctuations in the control system [5]. From the above, it is necessary to avoid the excessive adjustment during the motion to enhance the driving force coordination of the manipulator.

III. PARAMETERIZED TRAJECTORIES WITH B-SPLINE CURVES

The B-spline curve has the characteristics of local modification, convex hull, and continuous derivative, which makes

trajectories planned using the B-spline curve to exhibit continuity and geometric invariance. Therefore, in this paper, the trajectory of the end-effector of the manipulator in the Cartesian space is defined using the B-spline curves.

A k -order B-spline curve with $n + 1$ control points is typically defined as follows:

$$p(u) = \sum_{i=0}^n d_i \cdot N_{i,k}(u) \quad \left\{ \begin{array}{l} N_{i,0} = \begin{cases} 1 & u_i \leq u \leq u_{i+1} \\ 0 & \text{otherwise} \end{cases} \\ N_{i,k}(u) = \frac{u-u_i}{u_{i+1}-u_i} N_{i,k-1}(u) + \frac{u_{i+k+1}-u}{u_{i+k+1}-u_{i+1}} N_{i+1,k-1}(u) \\ \begin{matrix} 0 \\ 0 \end{matrix} = 0, \end{array} \right. \quad (13)$$

where $d_i (i = 0, 1, \dots, n)$ denotes the $n + 1$ control points, $u = [u_0, u_1, \dots, u_{n+k+1}]$ denotes the node vector of the k -order B-spline trajectory curve, and $N_{i,k}(u) (i = 0, 1, \dots, n)$ denotes the i th basis function of degree k . Additionally, the r -order differential $p^{(r)}(u)$ at point $p(u)$ on the k -order B-spline curve can be calculated as follows.

$$p^{(r)}(u) = \sum_{i=0}^{n-r} d_i^{(r)} \cdot N_{i,k-r}(u), \quad (14)$$

with:

$$d_i^{(r)} = \begin{cases} d_i & r = 0 \\ \frac{k-r-1}{u_{i+k+1}-u_{i+r}} (d_{i+1}^{(r-1)} - d_i^{(r-1)}) & r > 0, \end{cases} \quad (15)$$

The B-spline curve of k -order function is $k-2$ times continuously differentiable from (15), so the jerk continuous trajectory should be defined using B-spline curves with a degree no less than five. Considering the precision of the trajectory and calculation efficiency, a fifth-order B-spline curve with eleven control points is eventually selected to express the end-effector trajectory of the manipulator as follows:

$$p(u) = \sum_{i=0}^{10} d_i^p \cdot N_{i,5}(u), \quad (16)$$

where $d_i^p = [d_{ix}^p, d_{iy}^p, d_{iz}^p]$.

The end-effector of the manipulator is required to start or stop with zero linear velocity and acceleration from any initial pose point and stop at the target pose during actual operation. Therefore, the first three and last three control points must be consistent with the initial pose vector and the target pose vector, respectively.

$$\begin{aligned} d_0^p &= d_1^p = d_2^p = [p_x^i, p_y^i, p_z^i]^T, \\ d_8^p &= d_9^p = d_{10}^p = [p_x^f, p_y^f, p_z^f]^T, \end{aligned} \quad (17)$$

The remaining control points $\{d_3^p, d_4^p, d_5^p, d_6^p, d_7^p\}$ are generated using a data interval mapping method, whereby the randomly generated point coordinates are mapped to a

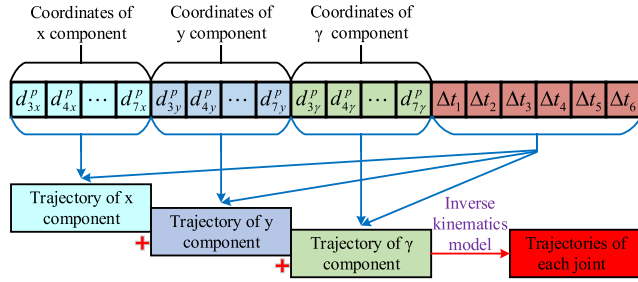


FIGURE 4. Parametric expression of end-effector trajectory.

data interval determined by the initial posture and the target posture. Assuming the randomly generated point coordinate is W_n^p , the coordinate of the i th original control point D_i^p is expressed as:

$$D_i^p = \sum_{n=3}^i W_n^p, \quad (i = 3, 4, \dots, 8), \quad (18)$$

After mapping according to the data interval, the coordinates of the i th control point of the motion track can be obtained as follows:

$$d_i^p = P_0 + \frac{D_i^p}{D_8^p} (P_e - P_0) \quad (i = 3, 4, \dots, 7)$$

$$d_3^p \leq d_4^p \leq d_5^p \leq d_6^p \leq d_7^p, \quad (19)$$

In addition, the first and last control points of the curve can be reached while the first and last node vectors of the clamped B-spline curve are repeated $k + 1$ times. The time node u_i can be normalized according to the cumulative chord length parameterization method, and the node vector can be obtained as follows:

$$\begin{cases} u_0 = u_1 = \dots = u_k = 0 \\ u_i = u_{i-1} + \frac{|\Delta t_{j-k-1}|}{\sum_{j=0}^{n-1} |\Delta t_j|} \quad (i = k + 1, \dots, n + k - 1) \\ u_{n+k} = u_{n+k+1} = \dots = u_{n+2k} = 1, \end{cases} \quad (20)$$

where $\Delta t_i = t_{i+1} - t_i$.

After the above steps, the motion trajectory of the end-effector can be parametrically expressed by the control points $\{d_3^p, d_4^p, d_5^p, d_6^p, d_7^p\}$ and time nodes $\{\Delta t_1, \Delta t_2, \Delta t_3, \Delta t_4, \Delta t_5, \Delta t_6\}$ as variables. Therefore, with the same time-node vectors, a motion trajectory of the pose components x , y , and γ of the end-effector can be constructed from the initial pose to the target pose using the B-spline curve through this parameterized trajectory. Subsequently, the trajectories of the joint are obtained using the inverse kinematics model. FIGURE 4 shows a diagram that intuitively depicts the parameterized trajectory.

IV. TRAJECTORY PLANNING OPTIMIZATION

For redundantly actuated parallel manipulators used in building construction, the trajectory planning of the end-effector

needs to be devised considering multiple tasks. For example, when the manipulator is used in building construction, the system stability must be given priority considering that the load is generally high during construction. The work efficiency is another important indicator given the numerous tasks in building construction. In addition, the actuators and degrade the tracking performance of the trajectory may be seriously damaged because of the vibrations due to non-smooth trajectories, so the smoothness of the motion trajectory is another important indicator to reduce vibrations, which may lead to considerable wear of the mechanical structures of the manipulator. Based on the above analysis, the driving force coordination ability, total exercise time, and maximum absolute value of each jerk of the actuator [25] are defined as objective functions to realize the optimization of the stability of the mechanism system, the work efficiency, and the smoothness of the motion respectively.

A. MATHEMATICAL MODEL OF MULTI-OBJECTIVE OPTIMAL TRAJECTORY

For redundantly driven parallel manipulators, improving the coordination of the driving forces will effectively reduce the internal forces of the manipulator and enhance its system stability. The norm $\|(\mathbf{J}_N)^{-T} (\mathbf{J}_R)^T\|$ average value of n pose points on the motion trajectory of the end-effector is selected to evaluate the driving force coordination of the manipulator through a dynamic analysis. Its expression is shown below:

$$M = \sum_{i=1}^n \left(\left\| (\mathbf{J}_N)^{-T} (\mathbf{J}_R)^T \right\|_i \right) / n, \quad (21)$$

Secondly, the total motion time, which is closely related to the work efficiency of the manipulator, can be calculated using the time node, which can be expressed as:

$$t_{total} = \sum_{i=1}^6 \Delta t_i, \quad (22)$$

Finally, the maximum absolute value of each jerk of the joint can be obtained using (4), which can be expressed as:

$$N = \max \{|J_i|\}, \quad (23)$$

In addition, considering the constraints of the angular displacement, angular velocity, and angular acceleration of each joint of the manipulator, a mathematical model of the multi-objective optimal trajectory can be established as follows. Notably, considering that the manipulator adopts a hybrid force and position control, the trajectory of the end-effector is only related to the three joints that are in the position control mode, so the speed and acceleration of only these joints are restricted.

$$\min F(x) = (f_1(x), f_2(x), f_3(x))$$

$$f_1(x) = M = \sum_{i=1}^n \left(\left\| (\mathbf{J}_N)^{-T} (\mathbf{J}_R)^T \right\|_i \right) / n$$

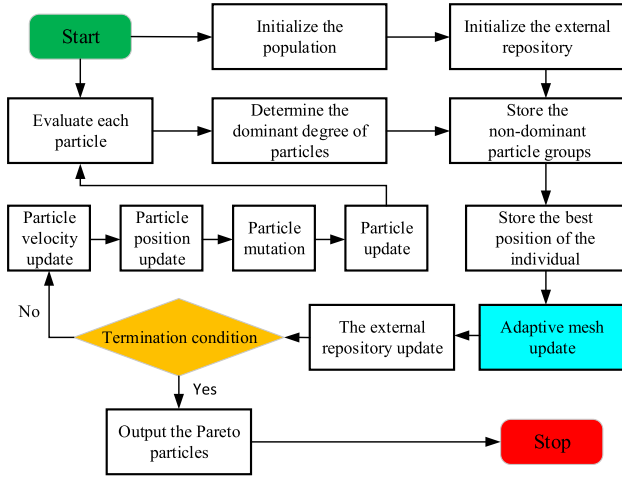


FIGURE 5. Calculation process of MOPSO.

$$\begin{aligned}
 f_2(x) t_{total} &= \sum_{i=1}^6 \Delta t_i f_3(x) = \max \{|J_i|\} \\
 &s.t. |\theta_i| \leq |\theta_i(P)|_{\max} \\
 |v_j| &\leq |\dot{\theta}_j(P, \dot{P})|_{\max} \\
 |a_j| &\leq |\ddot{\theta}_j(P, \dot{P}, \ddot{P})|_{\max} \quad (i = 1, 2, \dots, 6; j = 4, 5, 6)
 \end{aligned} \tag{24}$$

B. MULTI-OBJECTIVE OPTIMIZATION MODEL SOLUTION BASED ON MOPSO

A multi-objective optimization problem will require optimizing two or more functions simultaneously. For this type of problem, the different objectives have a trade-off relationship, so there is no single optimal solution but a set of optimal solutions called the Pareto-optimal solution or non-inferior solution. Common optimization algorithms include the MOGA, NPGA, PAES, and NSGA-II, and on this basis, for the trajectory optimization problem, a variety of optimization models are derived to effectively improve the algorithm performance [26]–[28]. In this paper, from the perspective of the solution convergence and diversity, the MOPSO algorithm proposed by Coello et al. [29], which has shown outstanding performance, is used.

The PSO algorithm is a population-based search algorithm based on the simulation of the social behavior of birds in a flock, which is the basis of the MOPSO algorithm [30]. The MOPSO algorithm is mainly composed of the maintenance of external repository, the selection of the best global position, and the updation of the best individual position. FIGURE 5 shows the calculation process of the MOPSO in solving a multi-objective optimal trajectory planning problem.

The main steps of the MOPSO algorithm are as follows:

Step 1: Initialize the population, set the number of iterations as $i = 1$, and combine the control point coordinates and time nodes in the B-spline parameter curve as one particle. Randomly generate N particles in the variable decision space and input the initial particle velocity. At the same time, set the maximum number of iterations and population size.

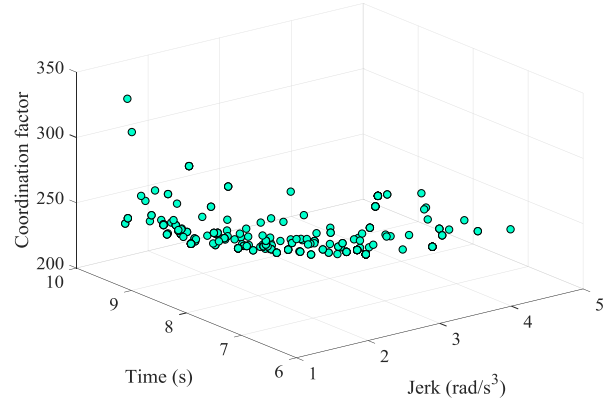


FIGURE 6. Pareto optimal fronts obtained from MOPSO.

Step 2: Evaluate each particle. Based on the B-spline trajectory constructed by the particles, determine whether to meet the constraints of (24), turn to Step 3 if it is satisfied. Otherwise, keep the particle in an infeasible solution set.

Step 3: Initialize the external repository. Calculate the three objective function values corresponding to each particle, store the positions of the particles that represent the non-dominated vectors in the non-dominant particle groups. The loops will start from Step 4 to Step 6 to update the population.

Step 4: Particle velocity update. The velocity of each particle is updated based on the following:

$$\begin{aligned}
 V(i + 1) &= w \cdot V(i) + r_1 \cdot c_1 \cdot [Pbest(i) - P(i)] \\
 &+ r_2 \cdot c_2 \cdot [REP(h) - P(i)],
 \end{aligned} \tag{25}$$

where $REP(h)$ is chosen from the roulette wheel selection.

Step 5: Particle position update. Update the position of each particle based on the following:

$$P(i + 1) = P(i) + V(i + 1), \tag{26}$$

If a particle travels outside the bounds, multiply the velocity by -1 .

Step 6: Particle mutation. Mutate every particle to obtain a new population.

Step 7: The external repository update. Update the non-dominated particle groups based on the density adaptive mesh method, and at the same time update the best position of the individual. After the non-dominated set reaches the upper storage limit, relatively sparse particles are retained based on the distribution density of the particles.

Step 8: Judge the termination condition. If the algorithm does not reach the maximum number of iterations, set $i = i + 1$. Otherwise, stop searching.

Step 9: Take the external repository as the Pareto optimal solution set.

V. NUMERICAL SIMULATION

To obtain the optimal trajectory of the end-effector, the multi-objective optimization model is solved using the MOPSO algorithm implemented in the MATLAB software.

TABLE 1. Lengths of each component of the manipulator.

Component	L ₁	L ₂	L ₃	L ₄	a	h
Length (mm)	1200	1202	1000	856	643	302

TABLE 2. Limits of the displacement of the manipulator joints.

Joint Angle	θ_1	θ_2	θ_3	θ_4	θ_5	θ_6
Lower Bound (rad)	0.70	0.70	0.52	0.52	1.05	0.52
Upper Bound (rad)	2.61	2.61	2.09	2.49	2.89	1.85

TABLE 3. Velocity and acceleration limits of non-redundantly actuated joints.

Joint No.	Velocity Limit (rad/s)	Acceleration Limit (rad/s ²)
4	5	2
5	5	2
6	5	2

TABLE 4. Optimal trajectory parameters.

Par.	Num.1	Num.2	Num.3	Num.4	Num.5	Num.6	Num.7	Num.8	Num.9	Num.10
d_{3x}^p	387.356	437.249	432.376	430.521	432.392	430.855	432.353	435.450	432.280	427.970
d_{4x}^p	466.017	523.040	504.592	524.000	522.844	518.369	519.674	518.229	514.354	510.906
d_{5x}^p	514.260	614.842	597.935	625.188	612.761	609.350	612.199	614.867	609.360	611.163
d_{6x}^p	599.681	722.431	694.531	717.308	714.811	711.348	715.285	705.203	703.960	715.908
d_{7x}^p	631.852	802.667	789.916	785.978	797.502	799.132	801.605	791.305	789.810	805.517
d_{3y}^p	1543.908	1583.282	1593.752	1575.148	1576.249	1574.090	1580.041	1576.174	1586.497	1583.856
d_{4y}^p	1522.338	1508.378	1550.994	1506.920	1512.092	1522.170	1512.442	1545.199	1537.428	1521.850
d_{5y}^p	1453.282	1485.057	1503.686	1464.824	1479.601	1483.155	1480.028	1506.222	1502.479	1484.073
d_{6y}^p	1448.836	1420.516	1462.236	1425.429	1431.956	1437.121	1428.214	1464.981	1459.397	1437.866
d_{7y}^p	1386.903	1364.441	1395.314	1367.996	1365.577	1372.610	1366.896	1383.590	1384.503	1367.600
d_{3y}^v	0.314	1.352	1.233	1.279	1.123	1.121	1.144	1.337	1.116	1.097
d_{4y}^v	0.458	3.319	2.667	3.329	3.008	2.878	3.024	3.183	2.773	2.817
d_{5y}^v	1.475	5.867	5.633	6.138	5.557	5.583	5.611	5.793	5.434	5.527
d_{6y}^v	6.890	8.977	8.196	8.723	8.424	8.297	8.508	8.306	8.159	8.338
d_{7y}^v	8.692	10.697	10.401	10.774	10.496	10.490	10.514	10.568	10.366	10.469
Δt_1	1.842	0.954	1.390	1.519	0.980	1.056	0.853	1.366	1.013	0.898
Δt_2	2.022	1.032	1.151	1.920	1.182	1.182	1.282	1.648	1.340	1.020
Δt_3	1.228	1.502	2.174	1.238	1.613	1.719	1.409	1.915	1.898	1.480
Δt_4	1.472	1.726	1.597	1.056	1.729	1.686	1.619	1.388	1.654	1.643
Δt_5	1.467	0.750	1.685	1.069	1.187	1.396	1.178	1.481	1.401	1.039
Δt_6	1.755	0.673	1.378	1.516	0.846	0.860	0.739	1.293	1.123	0.980

A. CONFIGURATION OF THE PARAMETERS

Table 1 lists the lengths of each component of the manipulator. The limits of the displacement, velocity, and acceleration of the manipulator joints are used as listed in Tables 2 and 3.

We assume that the motion of the end-effector starts from $\mathbf{P}_i = [350 \ 1640 \ 0^\circ]^T$ in the workspace with zero velocity and acceleration to the end point $\mathbf{P}_f = [850 \ 1320 \ 12^\circ]^T$, and stops there. At this time, the maximum motion time is set as 10 s.

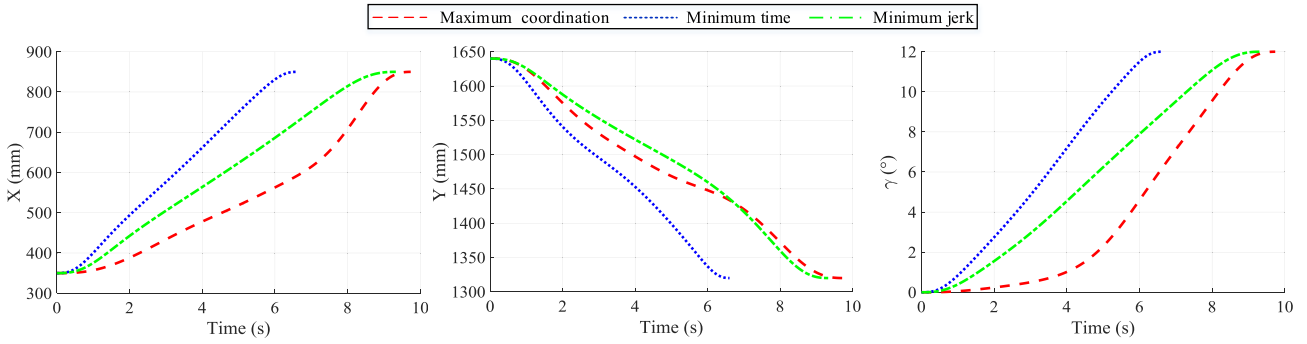


FIGURE 7. Trajectories of the pose components under a single optimal objective.

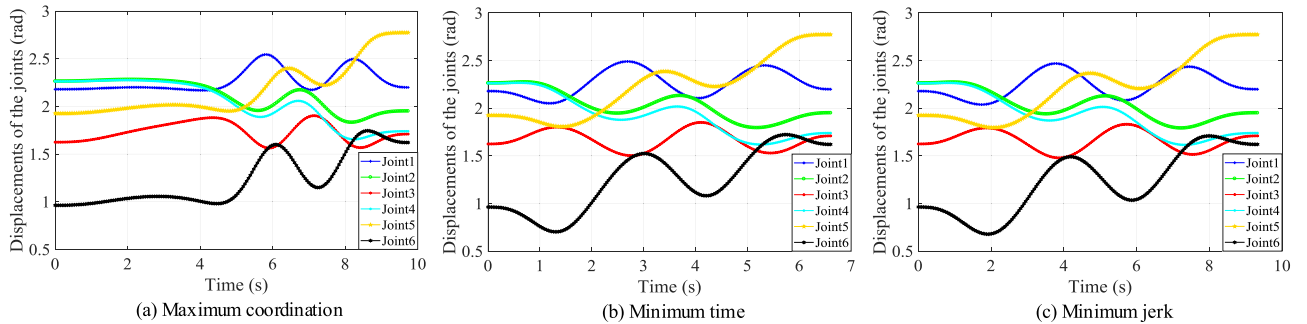


FIGURE 8. Displacements of six joints under a single optimal objective.

A multi-objective trajectory optimization is carried out using the MOPSO. The parameters of the MOPSO are set as follows: The initial population size is 200, and the maximum iteration number is 300. The learning factor C_1 is 0.1, and C_2 is 0.2. The inertia weight w is linearly decreased from 0.5 to 0.001, and the mutation probability is 0.1.

B. RESULTS AND DISCUSSION

A total of 133 groups of Pareto solutions are obtained using the MOPSO under 500 iterations. FIGURE 6 shows the distribution of the optimal Pareto front of the three objectives. As shown, the motion efficiency and motion stationarity represent two conflicting performance indicators, whereas the driving force coordination is relatively stable. Moreover, the three objectives can be efficiently balanced using the MOPSO from a given Pareto front result.

Ten groups of solutions are selected, as listed in Table 3, to facilitate the analysis. Each of these solutions is a sequence of 21 parameters that define a B-spline curve trajectory. Table 4 lists the corresponding values of the multi-objective functions. The optimal solutions that yield the maximum driving force coordination, minimum motion time, and minimum absolute value of the jerk are presented in columns 1, 2, and 3 of Table 4, respectively. The optimization results corresponding to the multi-objective functions are listed in columns 1, 2, and 3 of Table 5.

Based on the corresponding B-spline curve parameters of a single optimal objective, the motion trajectories of the pose vector components x , y , and γ of the end-effector can be obtained, as shown in FIGURE 7.

TABLE 5. Solutions of Pareto optimal front.

Obj.	M	$t_{total}(s)$	$ J^{max} (rad/s^2)$
sol.1	224.6208	9.7860	3.8308
sol.2	245.8504	6.6381	4.0252
sol.3	245.4118	9.3743	1.2427
sol.4	231.7327	8.3183	2.0612
sol.5	242.3796	7.5369	2.3470
sol.6	247.6821	7.8992	1.9904
sol.7	256.3012	7.0790	2.8580
sol.8	264.2579	9.0920	1.5860
sol.9	264.7652	8.4289	1.6774
sol.10	272.1076	7.0601	2.9200

The motion trajectories of each joint can be obtained using the inverse kinematics model. FIGURE 8 shows the displacements of six joints under a single optimal objective. FIGURE 9 shows the velocity and acceleration curves of three non-redundantly actuated joints. Evidently, the values of the displacement, velocity, and acceleration are within the upper and lower limits defined in Tables 2 and 3.

Based on the presented results, FIGURE 7 shows that the end-effector exhibits the fastest possible displacement under the minimum time trajectory whereas the smoothest motion under the minimum jerk trajectory. The manipulator has the highest motion efficiency when the motion time is minimum, i.e., 6.6381 s; however, the maximum absolute value of the jerk is as high as 4.0252 rad/s³.

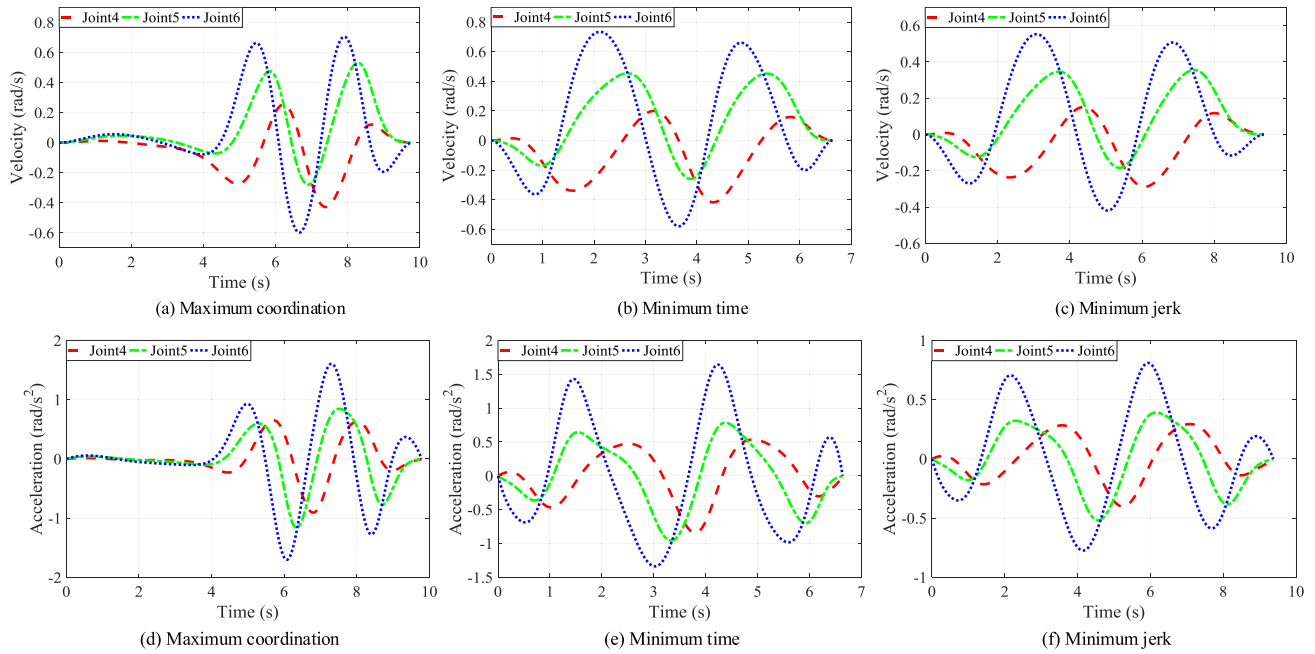


FIGURE 9. Velocity and acceleration curves of non-redundantly actuated joints under a single optimal objective.

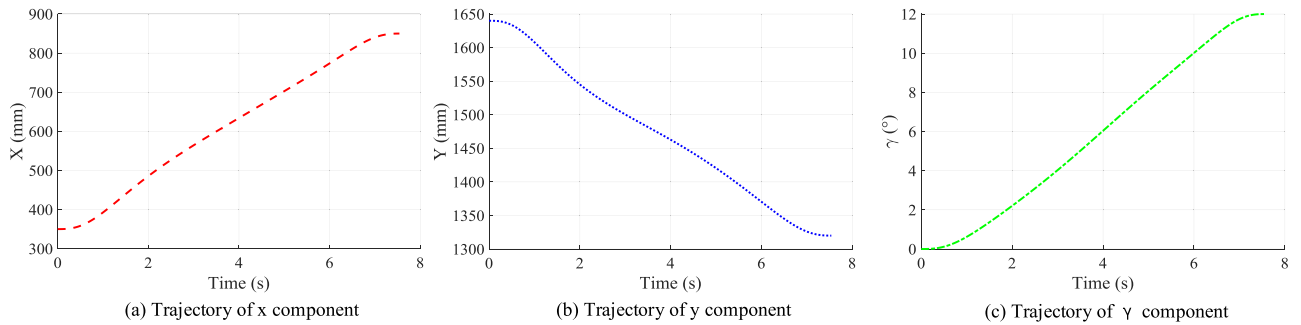


FIGURE 10. Comprehensive optimal trajectory of each pose component.

On the contrary, the manipulator has the highest motion stability when the maximum absolute value of the jerk is 1.2427 rad/s^3 ; however, the total motion time is relatively high at 9.3743 s . In addition, when the manipulator has the maximum driving force coordination, its motion time reaches a maximum of 9.7860 s because of a slow start of the end-effector, and the maximum absolute value of the jerk reaches 3.8308 rad/s^3 . Although the best driving force coordination of the manipulator can be guaranteed at this time, the other two objectives are far from ideal.

To meet the requirements of tasks and weaken the impact of conflicts between the objective functions, a fuzzy membership function for the comprehensive analysis of the weight of each objective is constructed as follows to obtain a potential optimal solution.

$$\max u_p = (\omega_1 \cdot u_1 + \omega_2 \cdot u_2 + \omega_3 \cdot u_3) / 3 \quad (27)$$

where ω_i is the weight of each objective, $u_1 = (f_{1\max} - f_1) / (f_{1\max} - f_{1\min})$, $u_2 = (f_{2\max} - f_2) / (f_{2\max} - f_{2\min})$, and $u_3 = (f_{3\max} - f_3) / (f_{3\max} - f_{3\min})$. In this paper, to prioritize the driving force coordination of the manipulator, the following

parameters are set: $\omega_1 = 0.4$, $\omega_2 = 0.3$, and $\omega_3 = 0.3$. Substituting the objective function values corresponding to the 118 groups of non-inferior sets obtained using the MOPSO algorithm into (27), a comprehensive optimal solution set is obtained as follows:

$$\begin{aligned} d_{jx}^p &= [880.254, 984.427, 1094.777, 1168.614, 1242.535] \\ d_{jy}^p &= [1384.128, 1460.560, 1516.994, 1584.750, 1607.335] \\ d_{j\gamma}^p &= [0.829, 2.241, 4.199, 6.285, 8.190] \\ &(j = 3, 4, \dots, 7) \\ \Delta t_i &= [7.883, 6.253, 4.666, 2.706, 8.242, 8.306] \\ &(i = 1, 2, \dots, 6) \end{aligned}$$

Based on this parameter, FIGURE 10 shows the comprehensive optimal motion trajectory of the pose components x , y , and γ of the end-effector. The three objectives (and their values) corresponding to this curve are the driving force coordination index (232.9347), exercise time (7.5786 s), and maximum absolute value of the jerk (2.4206 rad/s^3). Compared with the best situation of a single target, the difference

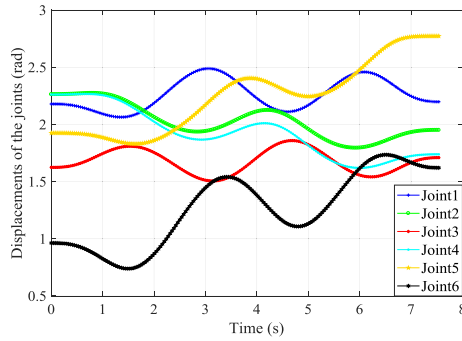


FIGURE 11. Displacements of six joints of the comprehensive optimal solution.

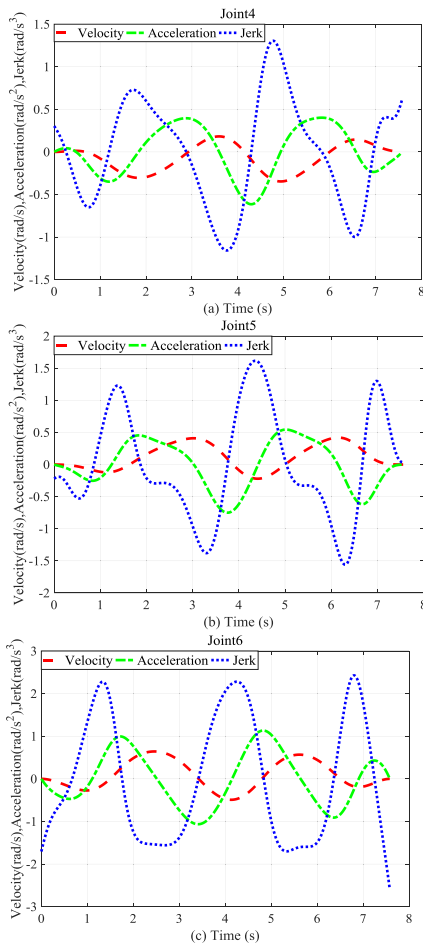


FIGURE 12. Trajectories of non-redundantly actuated joints of the comprehensive optimal solution.

between the driving force coordination evaluation factor is only 8.3139, the total motion time difference is 0.9405 s, and the maximum absolute value of the jerk difference is 1.1779 rad/s³. While ensuring better driving force coordination, the motion time and jerk are both in a relatively average range, which can effectively balance the optimization conflict between these objectives. FIGURE 11 shows the displacements of the six joints of the comprehensive optimal solution. FIGURE 12 shows the velocity, acceleration, and jerk curves of three non-redundantly actuated joints.

As depicted in FIGURES 11 and 12, the motion trajectories of the joints vary smoothly, and their physical parameters are within the ranges defined in Tables 2 and 3. The velocity and acceleration trajectories of the non-redundantly actuated joints both start and end at zero, as shown in FIGURE 12, thus ensuring a smooth start and stop of the manipulator. However, the jerk trajectories of the non-redundantly actuated joints do not start or end at zero; this can be solved by increasing the repetition of the initial point and the target point to four times. Notably, the curves can be further optimized if the number of control points or the degree of the B-spline curve is further increased. In summary, the simulation results confirm that the trajectory planning method can effectively produce a comprehensive optimal trajectory of the end-effector of the manipulator, thus proving the feasibility of this approach for redundantly actuated parallel manipulators. However, there are also cases where the program runs slowly due to the complexity of the optimization model, 500 iterations take about an hour, is quite a long-time process, and the number of Pareto sets is small. By further optimizing the program, the performance of this trajectory planning method can be improved.

VI. CONCLUSION

A multi-objective trajectory planning method for redundantly actuated parallel manipulators was developed in this study. Considering the control characteristics and actual work requirements of a redundantly actuated parallel manipulator, combined with the internal relationship between the motion trajectory and the driving force coordination of the manipulator, a mathematical model of the multi-objective optimal trajectory was established. The optimization model was solved using the multi-objective particle swarm optimization algorithm, and the potential optimal solution was obtained by constructing a comprehensive optimal evaluation method. The simulation results showed that the method is feasible and effective, as it can obtain an optimal trajectory that satisfies the work requirements while meeting the manipulator constraints. Moreover, the method is quite versatile in that it can provide a reference for the trajectory planning of other redundantly actuated parallel manipulators.

REFERENCES

- [1] J. F. O'Brien and J. T. Wen, "Redundant actuation for improving kinematic manipulability," in *Proc. IEEE Int. Conf. Robot. Autom.*, May 1999, pp. 1520–1525.
- [2] M. A. Nahon and J. Angeles, "Force optimization in redundantly-actuated closed kinematic chains," in *Proc. Int. Conf. Robot. Autom.*, 1989, pp. 951–952.
- [3] J. A. Saglia, J. S. Dai, and D. G. Caldwell, "Geometry and kinematic analysis of a redundantly actuated parallel mechanism that eliminates singularities and improves dexterity," *J. Mech. Des.*, vol. 130, no. 12, pp. 1786–1787, Dec. 2008, doi: 10.1115/1.2988472.
- [4] Y. Zhao and F. Gao, "Dynamic performance comparison of the 8PSS redundant parallel manipulator and its non-redundant counterpart—The 6PSS parallel manipulator," *Mechanism Mach. Theory*, vol. 44, no. 5, pp. 991–1008, May 2009, doi: 10.1016/j.mechmachtheory.2008.05.015.
- [5] X. Liu, J. Yao, Y. Xu, and Y. Zhao, "Research of driving force coordination mechanism in parallel manipulator with actuation redundancy and its performance evaluation," *Nonlinear Dyn.*, vol. 90, no. 2, pp. 983–998, Oct. 2017, doi: 10.1007/s11071-017-3706-8.

- [6] X. Jiang and C. Gosselin, "Dynamic point-to-point trajectory planning of a three-DOF cable-suspended parallel robot," *IEEE Trans. Robot.*, vol. 32, no. 6, pp. 1550–1557, Dec. 2016.
- [7] J. Jahanpour, M. Motallebi, and M. Porghoveh, "A novel trajectory planning scheme for parallel machining robots enhanced with NURBS curves," *J. Intell. Robot. Syst.*, vol. 82, no. 2, pp. 257–275, May 2016.
- [8] L. Liu, C. Chen, X. Zhao, and Y. Li, "Smooth trajectory planning for a parallel manipulator with joint friction and jerk constraints," *Int. J. Control, Autom. Syst.*, vol. 14, no. 4, pp. 1022–1036, Aug. 2016, doi: [10.1007/s12555-014-0495-4](https://doi.org/10.1007/s12555-014-0495-4).
- [9] Ü. Dinçer and M. Çevik, "Improved trajectory planning of an industrial parallel mechanism by a composite polynomial consisting of Bézier curves and cubic polynomials," *Mechanism Mach. Theory*, vol. 132, pp. 248–263, Feb. 2019, doi: [10.1016/j.mechmachtheory.2018.11.009](https://doi.org/10.1016/j.mechmachtheory.2018.11.009).
- [10] H. Wang, H. Wang, J. Huang, B. Zhao, and L. Quan, "Smooth point-to-point trajectory planning for industrial robots with kinematic constraints based on high-order polynomial curve," *Mechanism Mach. Theory*, vol. 139, pp. 284–293, Sep. 2019, doi: [10.1016/j.mechmachtheory.2019.05.002](https://doi.org/10.1016/j.mechmachtheory.2019.05.002).
- [11] C. Liu, G.-H. Cao, Y.-Y. Qu, and Y.-M. Cheng, "An improved PSO algorithm for time-optimal trajectory planning of delta robot in intelligent packaging," *Int. J. Adv. Manuf. Technol.*, vol. 107, nos. 3–4, pp. 1091–1099, Mar. 2020, doi: [10.1007/s00170-019-04421-7](https://doi.org/10.1007/s00170-019-04421-7).
- [12] H. Liu, X. Lai, and W. Wu, "Time-optimal and jerk-continuous trajectory planning for robot manipulators with kinematic constraints," *Robot. Comput.-Integr. Manuf.*, vol. 29, no. 2, pp. 309–317, Apr. 2013, doi: [10.1016/j.rcim.2012.08.002](https://doi.org/10.1016/j.rcim.2012.08.002).
- [13] S. Kucuk, "Optimal trajectory generation algorithm for serial and parallel manipulators," *Robot. Comput.-Integr. Manuf.*, vol. 48, pp. 219–232, Dec. 2017, doi: [10.1016/j.rcim.2017.04.006](https://doi.org/10.1016/j.rcim.2017.04.006).
- [14] C.-T. Chen and T.-T. Liao, "A hybrid strategy for the time- and energy-efficient trajectory planning of parallel platform manipulators," *Robot. Comput.-Integr. Manuf.*, vol. 27, no. 1, pp. 72–81, Feb. 2011, doi: [10.1016/j.rcim.2010.06.012](https://doi.org/10.1016/j.rcim.2010.06.012).
- [15] M. R. Azizi and R. Khani, "An algorithm for smooth trajectory planning optimization of isotropic translational parallel manipulators," *Proc. Inst. Mech. Eng., Part C, J. Mech. Eng. Sci.*, vol. 230, no. 12, pp. 1987–2002, 2016, doi: [10.1177/0954406215588988](https://doi.org/10.1177/0954406215588988).
- [16] Y. Liu, C. Tan, H. Sun, and G. Chen, "Multi-objective trajectory optimization for space manipulator with multi-constraints," in *Proc. IEEE Int. Conf. Mechatronics Autom. (ICMA)*, Aug. 2015, pp. 1542–1547.
- [17] X. Shi, H. Fang, G. Pi, X. Xu, and H. Chen, "Time-energy-jerk dynamic optimal trajectory planning for manipulators based on quintic NURBS," in *Proc. 3rd Int. Conf. Robot. Autom. Eng. (ICRAE)*, Nov. 2018, pp. 44–49.
- [18] A. Khoukhi, L. Baron, and M. Balazinski, "Constrained multi-objective trajectory planning of parallel kinematic machines," *Robot. Comput.-Integr. Manuf.*, vol. 25, nos. 4–5, pp. 756–769, Aug. 2009, doi: [10.1016/j.rcim.2008.09.002](https://doi.org/10.1016/j.rcim.2008.09.002).
- [19] J. Huang, P. Hu, K. Wu, and M. Zeng, "Optimal time-jerk trajectory planning for industrial robots," *Mechanism Mach. Theory*, vol. 121, pp. 530–544, Mar. 2018.
- [20] D. Chen, S. Li, J. Wang, Y. Feng, and Y. Liu, "A multi-objective trajectory planning method based on the improved immune clonal selection algorithm," *Robot. Comput.-Integr. Manuf.*, vol. 59, pp. 431–442, Oct. 2019.
- [21] L. Tang, C. Gosselin, X. Tang, and X. Jiang, "Dynamic trajectory planning of planar two-dof redundantly actuated cable-suspended parallel robots," in *Proc. IEEE/RSJ Int. Conf. Intell. Robots Syst.*, Sep. 2014, pp. 3874–3879.
- [22] Q. C. Pham and O. Stasse, "Time-optimal path parameterization for redundantly-actuated robots (numerical integration approach)," *IEEE/ASME Trans. Mechatronics*, vol. 20, no. 6, pp. 3257–3263, Dec. 2015, doi: [10.1109/TMECH.2015.2409479](https://doi.org/10.1109/TMECH.2015.2409479).
- [23] H. Wen, M. Cong, G. Wang, W. Qin, W. Xu, and Z. Zhang, "Dynamics and optimized torque distribution based force/position hybrid control of a 4-DOF redundantly actuated parallel robot with two point-contact constraints," *Int. J. Control Autom. Syst.*, vol. 17, pp. 1293–1303, May 2019, doi: [10.1007/s12555-018-0429-7](https://doi.org/10.1007/s12555-018-0429-7).
- [24] J. Wu, J. Wang, L. Wang, and T. Li, "Dynamics and control of a planar 3-DOF parallel manipulator with actuation redundancy," *Mechanism Mach. Theory*, vol. 44, no. 4, pp. 835–849, Apr. 2009, doi: [10.1016/j.mechmachtheory.2008.04.002](https://doi.org/10.1016/j.mechmachtheory.2008.04.002).
- [25] K. J. Kyriakopoulos and G. N. Saridis, "Minimum jerk path generation," in *Proc. IEEE Int. Conf. Robot. Autom.*, Apr. 1988, pp. 364–369.
- [26] H. Peng, B. Chen, and Z. Wu, "Multi-objective transfer to libration-point orbits via the mixed low-thrust and invariant-manifold approach," *Nonlinear Dyn.*, vol. 77, nos. 1–2, pp. 321–338, Jul. 2014.
- [27] W. Wang and H. Peng, "A fast multi-objective optimization design method for emergency libration point orbits transfer between the Sun–Earth and the Earth–Moon systems," *Aerosp. Sci. Technol.*, vol. 63, pp. 152–166, Apr. 2017.
- [28] H. Peng and W. Wang, "Adaptive surrogate model based multi-objective transfer trajectory optimization between different libration points," *Adv. Space Res.*, vol. 58, no. 7, pp. 1331–1347, Oct. 2016.
- [29] C. A. C. Coello, G. T. Pulido, and M. S. Lechuga, "Handling multiple objectives with particle swarm optimization," *IEEE Trans. Evol. Comput.*, vol. 8, no. 3, pp. 256–279, Jun. 2004, doi: [10.1109/TEVC.2004.826067](https://doi.org/10.1109/TEVC.2004.826067).
- [30] J. Kennedy and R. Eberhart, "Particle swarm optimization," in *Proc. IEEE Int. Conf. Neural Netw.*, Nov./Dec. 1995, pp. 1942–1948.



JIANBIN FENG received the B.S. degree from the Hefei University of Technology, China, in 2017. He is currently pursuing the M.S. degree with the Hebei University of Technology. His main research interests include research of redundantly actuated parallel manipulator and optimization algorithm.



TIEJUN LI (Member, IEEE) received the B.S. degree from the Hebei Institute of Mechanical and Electrical Engineering, in 1990, and the Ph.D. degree from the Harbin Institute of Technology, in 1997. He is currently a Professor with the Hebei University of Technology. His main research interest includes intelligent perception of robot.



MING HAN is currently pursuing the Ph.D. degree with the School of Mechanical Engineering, Hebei University of Technology. His main research interests include robotics, mechanism, mechanism theory, and so on.



KAIWEN ZHENG received the B.S. degree from the Hebei University of Engineering, in 2017. He is currently pursuing the M.S. degree with the Hebei University of Technology. His main research interests include human-robot collaboration and intention perception.



DONG YANG received the B.S. degree from the Hebei University of Science and Technology, in 2005, and the M.S. and Ph.D. degrees from the Hebei University of Technology, in 2008 and 2013, respectively. He is currently a Lecturer with the Hebei University of Technology. His main research interest includes architectural robots and its key technology.

• • •